Research Article | Vol. 30, No. 19 / 12 Sep 2022 / Optics Express 34385

Optics EXPRESS

Transient absorption microscopy setup with multi-ten-kilohertz shot-to-shot subtraction and discrete Fourier analysis

ROBERT SCHWARZL,[1] PASCAL HEIM,[1] MANUELA SCHIEK,[2] DARIO GRIMALDI,[3] ANDREAS HOHENAU,[3] JOACHIM R. KRENN,[3] AND MARKUS KOCH[1,*]

[1] *Graz University of Technology, Institute of Experimental Physics, Petersgasse 16, 8010 Graz, Austria*
[2] *Johannes Kepler University Linz, LIOS & ZONA, Altenberger Str. 69, A- 4040 Linz, Austria*
[3] *University of Graz, Institute of Physics, Universitätsplatz 5, 8010 Graz, Austria*
[*] *markus.koch@tugraz.at*

Abstract: Recording of transient absorption microscopy images requires fast detection of minute optical density changes, which is typically achieved with high-repetition-rate laser sources and lock-in detection. Here, we present a highly flexible and cost-efficient detection scheme based on a conventional photodiode and an USB oscilloscope with MHz bandwidth, that deviates from the commonly used lock-in setup and achieves benchmark sensitivity. Our scheme combines shot-to-shot evaluation of pump–probe and probe–only measurements, a home-built photodetector circuit optimized for low pulse energies applying low-pass amplification, and a custom evaluation algorithm based on Fourier transformation. Advantages of this approach include abilities to simultaneously monitor multiple pulse modulation frequencies, implement the detection of additional pulse sequences (e.g., pump–only), and expand to multiple parallel detection channels for wavelength-dispersive probing. With a 40 kHz repetition-rate laser system powering two non-collinear optical parametric amplifiers for wide tuneability, we find that laser pulse fluctuations limit the sensitivity of the setup, while the detection scheme has negligible contribution. We demonstrate the 2-D imaging performance of our transient absorption microscope with studies on micro-crystalline molecular thin films.

Published by Optica Publishing Group under the terms of the Creative Commons Attribution 4.0 License. Further distribution of this work must maintain attribution to the author(s) and the published article's title, journal citation, and DOI.

1. Introduction

Transient absorption (TA) spectroscopy is a technique where dynamics of a system after photoexcitation are investigated by detecting the intensity change of a probe laser pulse as a function of time, typically with femtosecond resolution [1–4]. With laser beam diameters in the millimeter range, the technique can be used to examine homogeneous samples such as dissolved molecules in solution, amorphous solids and single crystals. Micro- and nanostructured systems, such as quantum dots, nanowires, or textured thin films, additionally require spatial resolution to resolve local variations of the investigated processes. In transient absorption microscopy (TAM) [5–10] the laser pulses are focused to few µm or less, often close to their diffraction limit, in order to provide spatial as well as temporal resolution; spatial modulation even allows sub-diffraction-limited resolutions [11].

In TA measurements, the change in optical density is recorded with the pump-probe technique in two consecutive steps. First, a probe pulse passes through the sample where some of its energy is absorbed; the remaining wavelength-dependent intensity $I_{\mathrm{pr}}(\lambda_{\mathrm{pr}})$ is then recorded at the detector. Second, femto- to picoseconds before the next probe pulse arrives, a pump pulse excites a certain fraction of the sample (c.f., Fig. 1). This dynamical alteration in state population

#466272 https://doi.org/10.1364/OE.466272
Journal © 2022 Received 15 Jun 2022; revised 17 Jul 2022; accepted 18 Jul 2022; published 6 Sep 2022

Optics EXPRESS

directly leads to a transient change in probe intensity $I_{\text{pu-pr}}(\lambda_{\text{pu}}, \lambda_{\text{pr}}, \Delta t)$, dependent on the pump- and probe wavelength (λ_{pu} and λ_{pr} respectively) and on the pump–probe time delay (Δt), which is again measured at the detector. The pump beam does not contain relevant information and is therefore discarded. The influence of a pump pulse on the probe pulse is represented by the transient absorbance ΔA, often given in orders of magnitude of optical density (OD). Equation (1) shows this dependency explicitely:

$$\Delta A(\lambda_{\text{pu}}, \lambda_{\text{pr}}, \Delta t) = -\log_{10}\left(\frac{I_{\text{pu-pr}}(\lambda_{\text{pu}}, \lambda_{\text{pr}}, \Delta t)}{I_{\text{pr}}(\lambda_{\text{pr}})}\right) = -\log_{10}\left(1 + \frac{\Delta I_{\text{pr}}(\lambda_{\text{pu}}, \lambda_{\text{pr}}, \Delta t)}{I_{\text{pr}}(\lambda_{\text{pr}})}\right). \quad (1)$$

The second half of the equation relates ΔA to the pump-induced alteration of the probe intensity, $\Delta I_{\text{pr}} = I_{\text{pu-pr}} - I_{\text{pr}}$, which is often stated in literature.

In transient absorption microscopy, the illuminated sample area is typically very small, in consequence of the high spatial resolution required for many samples. In order to avoid photodamage, low fluences are required, often resulting in long data acquisition times. A high sensitivity ΔA_{min} is therefore a fundamental requirement for an efficient TAM setup.

Within the past years, multiple approaches have been presented to tackle this problem. Lock-in amplifiers and high repetition rate laser oscillators are often utilized to resolve intensity changes down to $\frac{\Delta I_{\text{pr}}}{I_{\text{pr}}} = 1 \cdot 10^{-7}$ [9] (note that the absolute sensitivity mainly depends on the number of averaged pulses). Recently, a high repetition rate laser has been combined with a multi-wavelength line scanner to reach $\frac{\Delta I_{\text{pr}}}{I_{\text{pr}}} = 1 \cdot 10^{-6}$ [12]. By contrast, amplified laser systems provide a much higher pulse energy at lower repetition rates, which enable the use of optical parametric amplification to generate wavelength-tuneable pulses, or broad-band white light supercontinuua for probing. The sensitivity suffers from the lower repetition rate and lies typically in the range of $\frac{\Delta I_{\text{pr}}}{I_{\text{pr}}} \approx 1 \cdot 10^{-4}$.

In this publication, we present a detection scheme that deviates from the commonly used direct lock-in analysis of the photodetector signal. We demonstrate the feasibility of using a single photodiode followed by analog signal processing and digitizing at moderate sample rates of 10 MHz. We use a laser repetition rate of 40 kHz and a mechanical chopper to achieve shot-to-shot acquisition of pump-probe measurements. The digitized signal is analyzed by Fourier transformation. With this approach, we achieve a sensitivity of $\frac{\Delta I_{\text{pr}}}{I_{\text{pr}}} = 4.7 \cdot 10^{-5}$ for a 200 000 pulse measurement in 5 s with a beam diameter of 6 µm. With two non-collinear optical parametric amplifiers (NOPAs), we achieve wavelength-tuneability of both pump and probe pulses at a temporal resolution of 80 fs (FWHM, cross correlation). For a probe pulse energy above 5 pJ, the sensitivity turns out to be almost exclusively limited by the laser noise. This high sensitivity (signal-to-noise ratio) combined with the non-destructive interaction of low energy pulses make the presented setup a versatile tool to study the spatio-temporal properties of a wide range of modern materials, such as two-dimensional transition metal dichalcogenides [13]. To demonstrate these capabilities, we investigate dynamics in thin films of micro-structured organic molecular crystals, which are very sensitive to photodamage.

Compared to photodiodes with dedicated lock-in amplifier hardware, the advantages of our approach include (i) the ability to monitor multiple frequency components at once, allowing the determination of pump-probe and probe-only intensities with one detector, (ii) the option to extend the pulse sequence to pump-only background measurements or dump pulses, and (iii) enabling massive parallelization, e.g., for multi-wavelength detection, all without significant extra costs.

2. Experimental setup

Our TAM, sketched in Fig. 1, consists of a femtosecond pump–probe microscopy setup to achieve femtosecond temporal and micrometer spatial resolution, a home-built photodetector optimized

Optics EXPRESS

for very low pulse energies, and an analog-to-digital converter (ADC), all three of which are described in the following sections. Analysis of the digitized photodetector signal is achieved through digital Fourier transformation, as described in Section 3.

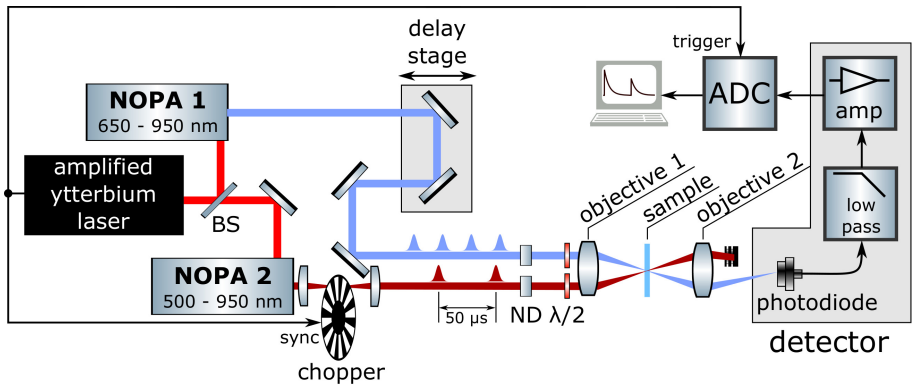

Fig. 1. Transient absorption microscope setup. Either of the two NOPAs can be used to generate the pump or probe pulses from the amplified ytterbium laser PHAROS PH1-20. The signal from the home-built photodetector is recorded using a PicoScope 5442A USB oscilloscope (ADC).

2.1. Femtosecond pump–probe microscope

We generate femtosecond laser pulses with an amplified Yb:KGW laser system (Light Conversion PHAROS PH1-20, 400 µJ pulse energy, 1025 nm central wavelength, ~270 fs pulse duration), operated at 40 kHz repetition rate. The pulses are evenly split to power two non-collinear optical amplifiers (both from Light Conversion, NOPA 1: ORPHEUS-N-2H, NOPA 2: ORPHEUS-N-3H). The accessible wavelength range stretches from 500/650 to 950 nm (c.f., Fig. 1) and prism compressors at the output of both NOPAs are used to obtain pulse durations of ≈30 fs at the sample. Operated at 40 kHz repetition rate, the setup provides relatively high pulse energies, that allow us to implement additional frequency doubling to reach a lower limit of 250 nm, or operate the system as a conventional TA spectrometer (without focusing) with white-light continuum generation in the probe path.

Because the laser pulse energy fluctuates with a strong correlation of successive laser pulses [14,15], which is known as $\frac{1}{f}$ noise, very rapid individual pump-probe measurements increase the signal-to-noise ratio. We therefore use a high-speed mechanical chopper (SciTec 310CD) to perform shot-to-shot measurements by blocking every other pump pulse. The pump beam is focused through the 0.76 mm broad slits of the chopping disk (SciTec 300CD200HS) whose rotational speed is synchronized to the pump laser at half the repetition rate. An individual pump-probe event is completed after two successive laser pulses, thus within 50 µs, and a measurement averages typically over a few seconds. The pump-probe delay can be set with a delay stage (motorized with a Newport LTA-HS actuator), providing a time-step resolution of 0.67 fs. The temporal resolution therefore depends almost only on the pulse duration. An intensity cross-correlation measurement yields a temporal resolution of 80 fs (FWHM) at 800 nm pump and probe wavelength. For some measurements, reflective or absorptive neutral density filters (ND), irises, achromatic $\lambda/2$ waveplates, or broadband wire grid polarizers are inserted into the pump and probe paths to adapt intensity and polarizations.

Both beams are spatially overlapped at the sample surface with a first microscope objective (Olympus UPlan FL N 10x, NA= 0.3), and transmitted light is collected with a second objective (Nikon Plan 10x, NA= 0.3) in confocal arrangement. The sample is located at the focal plane

Optics EXPRESS

and can be moved perpendicularly to the optical axis at micrometer precision with motorized translation stages (Thorlabs Z825B actuators). The transmitted pump beam can be blocked with a mechanical beam block in case of non-collinear pump- and probe beam paths, as in Fig. 1, and with spectral edge-pass or polarization filters in collinear setups. The probe light is guided onto the home-built photodetector and digitized, as described in the next section.

2.2. Photodetector

In order to detect transmission changes of the probe pulses with the highest possible sensitivity, we use a home-built photodetector, shown in Fig. 2. The detector is optimized for low laser pulse energies required in TAM. Additionally, it allows for low sample rates in the digitization process of the output signal by stretching the nanosecond voltage pulses from the photodiode into the 25 µs time window between two consecutive laser pulses [16]. The setup can easily be adapted to different repetition rates by changing the resistor and capacitor values and therefore the frequency response. We have chosen a photodiode (Hamamatsu, S1336-5BQ) with small capacitance ($C_{\mathrm{Pd}} = 65$ pF) in order to account for the low pulse energies in the range of 5 pJ, corresponding to only $\approx 3.2 \cdot 10^7$ photons per pulse (at 650 nm). With the photo diode's quantum efficiency of 70 %, the generated voltage pulses peak at about 17 mV (for 3 pJ pulses), before it decays with a time constant of $\tau_{\mathrm{Pd}} = C_{\mathrm{Pd}} R_{\mathrm{Pd}}$ ($R_{\mathrm{Pd}} \sim 10$ kΩ).

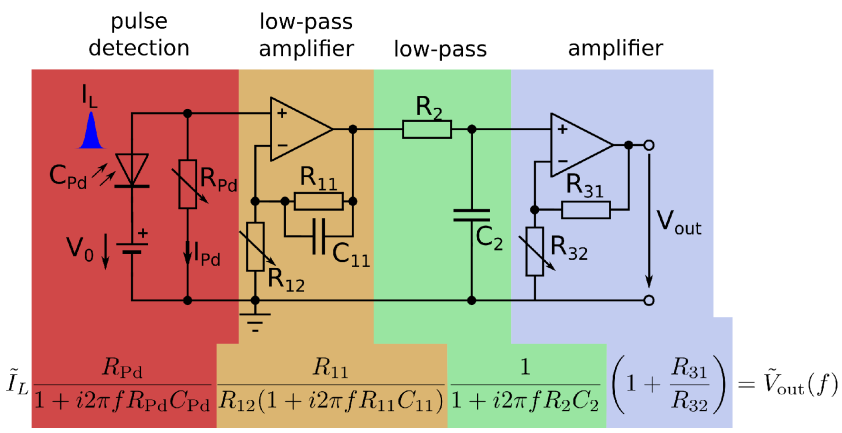

Fig. 2. Amplifier circuit schematic including the frequency response. I_L current produced by the light pulse which charges the capacity of the photodiode, V_{out} resulting voltage signal. See text for a description of the circuit. Frequency response: Eq. (2)

The voltage pulse is amplified and further stretched in time with a low-pass amplifier (yellow section in Fig. 2), using an operational amplifier (OP-AMP) with a capacitor (C_{11}) in parallel with the feedback resistor (R_{11}). We use an OP-AMP with high input impedance in order to separate the small photodiode current I_{Pd} from the rest of the circuit. Note that the voltage rise at R_{Pd} after laser pulse arrival proceeds very rapidly, so that the rise of the OP-AMP output voltage is limited to its slew rate. The duration of this nonlinear behavior lasts a few nanoseconds and is reduced by C_{11}, which lowers the amplification factor during this fast voltage change. A measurement of the transient voltage pulse after this active low pass is shown as a yellow line in Fig. 3(a). The pulse is then further stretched in time by a passive low-pass filter (green in Figs. 2 and 3(a)), and finally amplified by a second OP-AMP to match the input range of the analog-to-digital converter (purple in Figs. 2 and Fig. 3(a)).

The amplification function in the frequency domain is shown in Fig. 2 (Eq. (2)) with the same color coding as in the schematic, in order to highlight the contributions of the individual amplifier stages. The corresponding Bode plot in Figs. 3(b) and 3(c) shows the frequency response of the

Optics EXPRESS

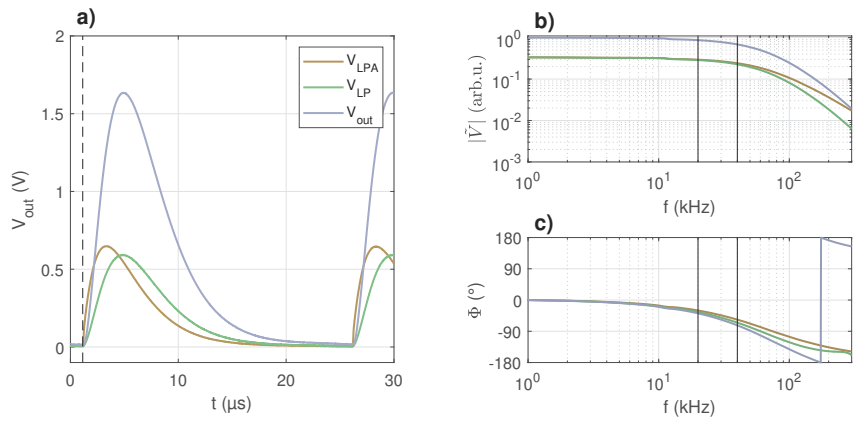

Fig. 3. Time- and frequency-domain behavior of the photodetector. **(a)** Voltage pulses at different stages of the amplifier. The dashed line indicates the arrival time of the laser pulse. The voltage at R_{Pd} is not shown because it cannot easily be measured due to the input impedance of the oscilloscope being too low. The orange and green curves show the stretched pulse shape after the first OP-AMP and after the low pass filter, respectively (see Fig. 2, similar color coding). The purple curve is the output voltage and represents the impulse response function $V(t)$ that characterizes the temporal behavior of the photodetector. **(b), (c)** Bode plot showing the frequency-dependent amplification (b) and phase shift (c) of the amplifier circuit. Vertical lines at 20 and 40 kHz indicate the chopping frequency and the laser repetition rate, respectively.

individual amplifier stages. For further analysis of the detected laser pulses in Chapter 3, we will use the impulse response function $V(t)$ of the output (purple line in Fig. 3(a)) in the time domain, and the frequency response function $\tilde{V}(f)$ (purple line in Fig. 3(b)) in the frequency domain.

2.3. Signal digitization

The advantage of our photodetector with its low-pass characteristics becomes apparent in the signal digitization stage, where a low-bandwidth and low-sampling-rate ADC suffices. We use a low-cost ADC (Picoscope 5442D) with 10 MS s^{-1} sample rate, 60 MHz bandwidth and 16 bit resolution, capable of recording up to 128 000 pump-probe events in sequence with its on-board memory of 128 MB. Due to the low-pass characteristic of our detector, the Nyquist rate is far below the sample rate, so that there is no risk for aliasing.

A typical measurement takes about 1 s, which leads to a frequency resolution (FWHM of $\tilde{S}(\Delta f)$, see below) of 1.2 Hz, further reducing the chance of aliasing problems.

3. Analysis of transient absorption microscopy measurements

In the following, we discuss the algorithm for computing the transient absorbance from the digitized signal. Analysis of the periodic, shot-to-shot TA measurements follows the basic idea of the Lock-In technique [17]. We modulate the pump pulses at half the laser repetition rate, $f_0/2 = 20$ kHz, by blocking every other pulse (c.f., Fig. 1). This creates a modulation with the same frequency of 20 kHz in the probe pulse intensity, so that every other probe pulse is increased or decreased in power. As the temporal width of the pump pulses is about 10^6 times shorter than the sampling period of the ADC, the detected laser intensity over time, $I_{\mathrm{L}}(t)$, can be approximated by a delta comb with the alternating amplitudes $I_{\text{pu-pr}}$ and I_{pr}, corresponding to the transmitted

Optics EXPRESS

probe intensity of pump–probe and the probe-only measurements:

$$I_{\mathrm{L}}(t) = \sum_{m=-\infty}^{\infty} \left\{ I_{\text{pu-pr}}\delta\left[\frac{2}{f_0}m - \left(t - T_0\right)\right] + I_{\text{pr}}\delta\left[\frac{2}{f_0}m - \left(t - T_0 - \frac{1}{f_0}\right)\right]\right\}, \tag{2}$$

where T_0 is a temporal offset adjustable using the pump laser's internal delay and m is an integer accounting for the signal periodicity. This periodic laser signal is detected with the photodetector, consisting of the photodiode and low-pass amplifier (see Fig. 2), and subsequently digitized. Thus the signal $S(t)$ can be described as convolution of the laser pulses $I_{\mathrm{L}}(t)$ with the impulse response function of the detector $V(t)$ (see Fig. 3):

$$S(t) = I_{\mathrm{L}}(t) \circledast V(t). \tag{3}$$

In the frequency domain, the signal spectrum $\tilde{S}(f)$ is obtained as product of the pulse spectrum $I_{\mathrm{L}}(f)$ with the frequency response function $\tilde{V}(f)$

$$\tilde{S}(f) = \tilde{I}_{\mathrm{L}}(f)\tilde{V}(f). \tag{4}$$

Due to the alternating intensity of the laser pulses arriving at the detector (Eq. (2)), corresponding to a $1/(2f_0)$ periodicity, the signal spectrum is discrete with a $f_0/2$ spacing (see Eq. (S2) in the supplementary information).

$$\tilde{S}\left(n\frac{f_0}{2}\right) = e^{i\phi_0 \frac{n}{2}}\tilde{V}\left(n\frac{f_0}{2}\right)\left[|\tilde{I}_{\text{pu-pr}}| + (-1)^n|\tilde{I}_{\text{pr}}|\right], \tag{5}$$

where n is an integer, $\phi_0 = 2\pi f_0 T_0$ corresponds to the temporal offset T_0. $|\tilde{I}_{\text{pu-pr}}|$ and $|\tilde{I}_{\text{pr}}|$ are proportional to the alternating amplitudes $I_{\text{pu-pr}}$ and I_{pr}, which we can determine from the two equations for $n = 1$ and 2:

$$n = 1 : \tilde{S}\left(\frac{f_0}{2}\right) = e^{i\frac{\phi_0}{2}}\tilde{V}\left(\frac{f_0}{2}\right)\left(|\tilde{I}_{\text{pu-pr}}| - |\tilde{I}_{\text{pr}}|\right), \tag{6}$$

$$n = 2 : \tilde{S}(f_0) = e^{i\phi_0}\tilde{V}(f_0)\left(|\tilde{I}_{\text{pu-pr}}| + |\tilde{I}_{\text{pr}}|\right). \tag{7}$$

$\left|\tilde{S}\left(\frac{f_0}{2}\right)\right|$ thus is proportional to the difference of two consecutive pulses, which is typically very small, while $\left|\tilde{S}(f_0)\right|$ is proportional to their sum. Since the detector influences both amplitude and phase in dependence of frequency, it is important to consider the frequency response function $\tilde{V}(f)$ for the two frequencies f_0 and $\frac{f_0}{2}$ (c.f., Fig. 3).

We define two detector-specific quantities. First, P_{f_0}, which has unit length and accounts for the phase shift induced by the detector at f_0:

$$P_{f_0} = \frac{\tilde{V}(f_0)^*}{|\tilde{V}(f_0)|}. \tag{8}$$

Second, $T_{\frac{f_0}{2}\to f_0}$ accounts for both gain difference and phase shift difference between f_0 and $\frac{f_0}{2}$:

$$T_{\frac{f_0}{2}\to f_0} = \frac{\tilde{V}(f_0)}{\tilde{V}(\frac{f_0}{2})}. \tag{9}$$

Both complex quantities, P_{f_0} and $T_{\frac{f_0}{2}\to f_0}$, are determined from the experiment and are constant for stable detector configurations (see section 3 in the supplementary information.)

Optics EXPRESS

With these quantities Eqs. (6) and (7) can be written as:

$$\tilde{S}\left(\frac{f_0}{2}\right) T_{\frac{f_0}{2}\to f_0} P_{f_0} e^{-i\frac{\phi_0}{2}} = \left|\tilde{V}(f_0)\right| \left(|\tilde{I}_{\text{pu-pr}}| - |\tilde{I}_{\text{pr}}|\right) =: \mathcal{S}\left(\frac{f_0}{2}\right), \tag{10}$$

$$\tilde{S}(f_0) P_{f_0} e^{-i\phi_0} = \left|\tilde{V}(f_0)\right| \left(|\tilde{I}_{\text{pu-pr}}| + |\tilde{I}_{\text{pr}}|\right) =: \mathcal{S}(f_0). \tag{11}$$

Note that $\mathcal{S}\left(\frac{f_0}{2}\right)$ and $\mathcal{S}(f_0)$ are a real-valued quantities because the phase shift induced by the detector is compensated by $T_{\frac{f_0}{2}\to f_0}$ and P_{f_0} and the phase induced by the time difference between the first pulse and $t = 0$ is compensated by ϕ_0. The phase shift ϕ_0 can be calculated in every measurement separately from

$$\tilde{S}(f_0) P_{f_0} = |\tilde{S}(f_0)| e^{i\phi_0}, \tag{12}$$

as

$$\phi_0 = \arccos\left\{\frac{\text{Re}\left[\tilde{S}(f_0) P_{f_0}\right]}{\left|\tilde{S}(f_0)\right|}\right\}. \tag{13}$$

The transient absorbance change ΔA, as defined in Eq. (1), can thus be calculated from the frequency-domain signals $\tilde{S}\left(\frac{f_0}{2}\right)$ and $\tilde{S}(f_0)$ with Eqs. (10) and (11):

$$\Delta A = -\log_{10}\left(\frac{I_{\text{pu-pr}}}{I_{\text{pu}}}\right) = -\log_{10}\left(\frac{|\tilde{I}_{\text{pu-pr}}|}{|\tilde{I}_{\text{pu}}|}\right) = -\log_{10}\left\{\frac{\text{Re}\left[\mathcal{S}(f_0) + \mathcal{S}\left(\frac{f_0}{2}\right)\right]}{\text{Re}\left[\mathcal{S}(f_0) - \mathcal{S}\left(\frac{f_0}{2}\right)\right]}\right\}. \tag{14}$$

Note that $\mathcal{S}(f_0)$ and $\mathcal{S}\left(\frac{f_0}{2}\right)$ in Eq. (10) and (11) have no imaginary part, but noise has. Therefore, by discarding the imaginary part, the signal-to-noise ratio is significantly improved.

The evaluation uses the phase and amplitude of certain frequencies. If a signal is sampled discretely in time, then the phase of the Fourier transform is very sensitive on the frequency f. In fact, a frequency change of $f \to f + \frac{1}{\Delta T}$, where ΔT is the sample time of the oscilloscope, leads to a phase shift of 2π. Therefore, it is crucial to evaluate the repetition rate f_0 in each measurement in order to compensate for slight drifts caused by external influences on the laser system. A method for determining repetition rate drifts is explained in section 2 of the supplementary information.

Section 4 of the supplementary information shows the extension of the data analysis method for arbitrarily many delta combs. This would allow measuring the pump-only background by modulating the pump and the probe pulses in order to make a pump-probe, pump-only and probe-only measurement.

4. Performance of the TAM setup

4.1. Dynamics in thin metal films: Sensitivity determination

We determine the sensitivity of our setup by measuring the picosecond dynamics of thin metal films. We use a thin film of 30 nm gold and 3 nm chromium deposited on a commercial ITO-coated microscopy slide (indium tin oxide). Similar measurements which also probe the transition from the d-band to the Fermi surface on gold thin films can be found in the literature [18]. They show that the contributing factors to the transient absorption signal are the thermalization of electrons through electron-electron interaction and electron-phonon interaction; with dominance of the latter on the ps timescale. Figure 4(a) shows the transient absorption obtained with pump pulses of 680 nm wavelength (1.82 eV photon energy), 275 pJ pulse energy and ≈1050 µJ cm^{-2} peak fluence, and probe pulses of 504 nm (2.46 eV), 30 pJ and ≈115 pJ cm^{-2}. Pulses of approximately 10 pJ are transmitted through the sample and recorded by the detector. The laser spot diameter

Optics EXPRESS

at the sample was 6 µm. In order to determine the signal fluctuations, we record a dataset of 1000 individual measurements at a pump-probe delay of 1.95 ps, each of which accumulates data for 0.5 s at 40 kHz repetition rate, corresponding to 10 000 probe-only and 10 000 pump-probe events. Figure 4(b) shows the individual transient absorption values and Fig. 4(c) a histogram of their relative abundance, which follows a normal distribution (red curve), as expected. The standard deviation of the data set is $\sigma(\Delta A) = 65$ µOD corresponding to $\frac{\Delta I_{pr}}{I_{pr}} = 1.5{\cdot}10^{-4}$ for a single 0.5 s measurement. Note that we have chosen relatively short data accquisition times of 0.5 s for this characterization measurement in order to reveal the signal fluctuations, determining the sensitivity. For a typical high-resolution measurement with an integration time of 5 s (200 000 laser pulses), the standard error reduces to 20 µOD corresponding to $\frac{\Delta I_{pr}}{I_{pr}} = 4.7{\cdot}10^{-5}$.

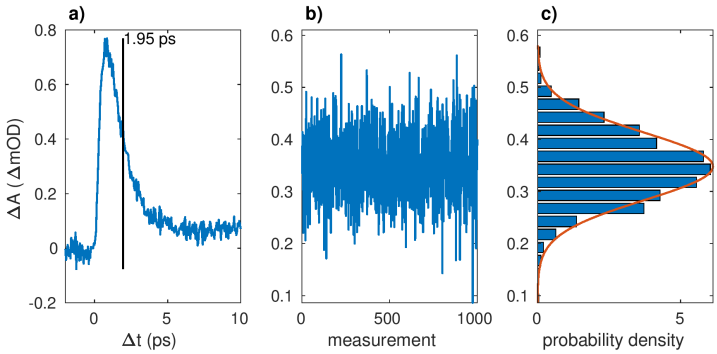

Fig. 4. Transient absorption measurement series of a thin metal film (integration time 5 s per point) for sensitivity determination. **(a)** Pump-probe delay scan. **(b)** Dataset of 1000 measurements at a constant pump-probe delay of 1.95 ps, with a data acquisition time of 0.5 s for each measurement. **(c)** Probability distribution of the data set shown in (b), following a Gaussian distribution with a standard deviation of 65 µOD corresponding to $\frac{\Delta I_{pr}}{I_{pr}} = 1.5{\cdot}10^{-4}$.

In order to identify the origin of these fluctuations, we compare the dataset to a simulation, explained in detail in section 5 of the supplementary information. This simulation is based on the pulse energy distribution collected with our photodetector by integrating over single pulses from the home-built photodetector at a repetition rate of 20 kHz. The reduced repetition rate avoids overlapping pulses in the digitized signal. The pulse energy distribution is in agreement with measurements generated from a Coherent LabMax pulse meter at 400 Hz. Based on the assumption of independent pump and probe pulses, the simulation predicts a larger standard deviation of $\sigma(\Delta A) = 111$ µOD corresponding to $\frac{\Delta I_{pr}}{I_{pr}} = 2.6{\cdot}10^{-4}$. This result indicates a pulse energy correlation of consecutive laser pulses, leading to reduced fluctuations in the shot-to-shot analysis. Importantly, this result also indicates that the sensitivity of our TAM is limited by pulse energy fluctuations of the NOPAs, and that the contribution to the fluctuations of our photodetector and evaluation algorithm are negligible. We note that we typically obtain lower fluctuations around the center of the NOPA tuning curve, where the device performance is more stable.

4.2. Exciton dynamics in micro-crystalline molecular thin films

We demonstrate the performance of our TAM with the investigation of micro-textured organic thin films. With a film thickness of ~50 nm resulting in a weak transient absorption, these molecular crystals require a high sensitivity. The sample under investigation consists of anilino squaraines with isobutyl side chains (SQIB) in its orthorhombic crystal structure. The samples are obtained on glass substrates by solution processing with subsequent thermal annealing to

Optics EXPRESS

induce crystallization into platelet-like rotational domains with preferred parallel orientation of a single crystallographic plane to the substrate. [19,20] The SQIB platelet size of about 100 µm and their characteristic linear polarized absobance pattern are well suited for microscopic optical investigations. The SQIB platelets are characterized by a pronounced Davydov splitting of the excited states into a lower Davydov component (LDC) at 1.68 eV (740 nm photoexcitation wavelength) and an upper Davydov component (UDC) at 1.91 eV (650 nm) [19]. The two Davydov components can be selectively excited due to this pronounced splitting, and because the transition dipole moments of the UDC and LDC are perpendicular, (for a full characterization of the biaxial dielectric tensor with imaging Mueller matrix ellipsometry see Ref. [20]). This results in a characteristic linear dichroism with two absorption maxima (UDC and LDC) polarized mutually perpendicular within the plane of a platelet. Since the platelets have a random rotational in-plane orientation, transmission of linearly polarized light with fixed wavelength and polarization direction results in different spatial absorbance patterns of each platelet. [20]

Here, we demonstrate that our TAM setup is capable to observe the ultrafast exciton dynamics within individual platelets. Figure 5 shows a TAM measurement with pump excitation to the UDC and probe absorption at the transition from the ground state to the LDC. We rotate the polarization direction of the pump beam in order to obtain maximum single-pulse absorbance in the chosen platelet. The probe beam is polarized perpendicularly to the pump. The transient absorption shown in Fig. 5(b) becomes instantly negative, then increases exponentially within about 10 ps and finally levels off at a slightly negative value. This transient behavior is indicative of immediate ground-state bleach followed by rapid and almost complete non-radiative population decay to the ground state, which is in agreement with the low fluorescence yield observed in static experiments [21].

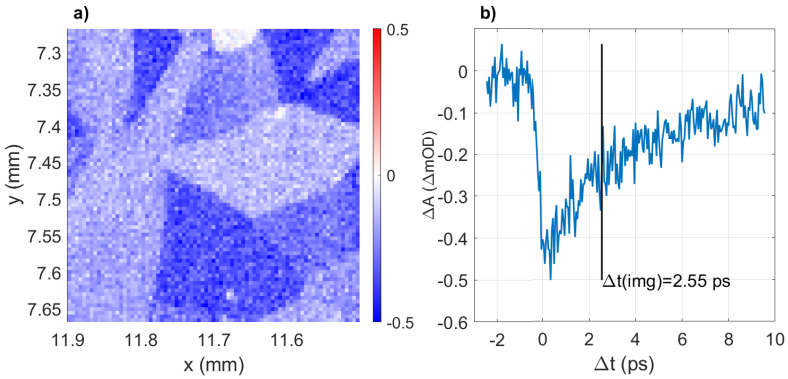

Fig. 5. TAM measurements of micro-textured orthorhombic SQIB, obtained by UDC excitation and time-delayed probing of the LDC band. Pump pulses (12.5 pJ) and probe pulses (6.3 pJ) are perpendicularly polarized. **(a)** TAM image recorded at 2.55 ps pump-probe delay with spatially fixed polarizations. **(b)** TA scan of a single platelet with optimized pump and probe polarization directions. For the image in (a), the transient absorbance ΔA without pump influence is subtracted from the pump-probe transient absorbance at 2.55 ps to remove stray pump light. The FWHM of the pump and probe beam is 4 µm.

A 2D image recorded with a fixed time delay of 2.55 ps is shown in Fig. 5(a). The individual platelets become visible, because the transient absorption signal ΔA depends on the relative orientation of the laser polarization and the UDC transition dipole moment of the platelets. This measurement indicates that the setup is also capable of polarization-resolved femtosecond microscopy by introducing $\frac{\lambda}{2}$ plates and polarizing optical elements.

The image shown in Fig. 5(a) consists of 6400 pixels (80 times 80) and was recorded within 96 minutes, with a data acquisition time of 0.5 s for each pixel and additional 0.4 s per pixel for

Optics EXPRESS

scanning the sample. The recording of a series of images with different delays is thus easily possible, enabled by the high sensitivity of the system.

5. Conclusion and outlook

We present a highly sensitive, flexible and yet cost-efficient detection scheme for transient absorption microscopy. A sensitivity of $\frac{\Delta I_{\mathrm{pr}}}{I_{\mathrm{pr}}} = 4.7{\cdot}10^{-5}$ corresponding to $\Delta A = 20\,\mu\mathrm{OD}$ is achieved using a Fourier transform based analysis algorithm. This algorithm is applied to alternating pump-probe and probe-only pulses recorded with a home-built photodetection system. The photodiode signal is amplified, low-pass filtered and recorded using a USB oscilloscope. Analysis of the digitized signal could alternatively be achieved with a software-based lock-in amplifier code [17]. Measurements indicate that the dominant source of noise is the femtosecond laser system, so further improvement in signal-to-noise ratio is possible with a more stable laser. Intensities as low as 10 pJ per pulse are sufficient to achieve this signal-to-noise ratio.

This setup allows us to investigate samples that are very sensitive to photodamage such as the textured squaraine organic thin films shown in Fig. 5. In the future, we plan to investigate population dynamics and higher excited states of prototypical micro-crystalline textured organic thin films from e.g. squaraines which are not accessible from the ground state. The detection algorithm allows to record arbitrary pulse trains from one or more channels at the same time. This is useful for pump-dump-probe setups, separate pump-only measurements and more. Wavelemgth-dispersive detection can be realized by implementing a diffraction grating combined with a photodiode array or a CCD linear image sensor. Read-out with the presented detection scheme through parallel channels enables a higher cost efficiency, compared to multiple lock-in amplifiers. Furthermore, a spatially separated pump-probe extension will provide insight into charge or energy propagation on the µm scale.

Funding. Austrian Science Fund (P 33166); Zukunftsfonds Steiermark; NAWI Graz; Linz Institute of Technology (LIT-2019-7-INC-313 SEAMBIOF).

Acknowledgements. PH, RS and MK acknowledge the financial support by Zukunftsfonds Steiermark, NAWI Graz, and the Austrian Science Fund (FWF) under Grant P 33166. MS thanks the Linz Institute of Technology (LIT-2019-7-INC-313 SEAMBIOF) for funding.

Disclosures. The authors declare no conflicts of interest.

Data availability. Data underlying the results presented in this paper are not publicly available at this time but may be obtained from the authors upon reasonable request.

Supplemental document. See Supplement 1 for supporting content.

References

1. U. Megerle, I. Pugliesi, C. Schriever, C. F. Sailer, and E. Riedle, "Sub-50 fs broadband absorption spectroscopy with tunable excitation: putting the analysis of ultrafast molecular dynamics on solid ground," Appl. Phys. B **96**(2-3), 215–231 (2009).
2. J. Cabanillas-Gonzalez, G. Grancini, and G. Lanzani, "Pump-probe spectroscopy in organic semiconductors: Monitoring fundamental processes of relevance in optoelectronics," Adv. Mater. **23**(46), 5468–5485 (2011).
3. K. E. Knowles, M. D. Koch, and J. L. Shelton, "Three applications of ultrafast transient absorption spectroscopy of semiconductor thin films: spectroelectrochemistry, microscopy, and identification of thermal contributions," J. Mater. Chem. C **6**(44), 11853–11867 (2018).
4. T. H. Lai, K. I. Katsumata, and Y. J. Hsu, "In situ charge carrier dynamics of semiconductor nanostructures for advanced photoelectrochemical and photocatalytic applications," Nanophotonics **10**(2), 777–795 (2020).
5. E. M. Grumstrup, M. M. Gabriel, E. E. Cating, E. M. Van Goethem, and J. M. Papanikolas, "Pump–probe microscopy: Visualization and spectroscopy of ultrafast dynamics at the nanoscale," Chem. Phys. **458**, 30–40 (2015).
6. M. C. Fischer, J. W. Wilson, F. E. Robles, and W. S. Warren, "Invited Review Article: Pump-probe microscopy," Rev. Sci. Instrum. **87**(3), 031101 (2016).
7. D. Davydova, A. de la Cadena, D. Akimov, and B. Dietzek, "Transient absorption microscopy: advances in chemical imaging of photoinduced dynamics," Laser Photonics Rev. **10**(1), 62–81 (2016).
8. T. Zhu, J. M. Snaider, L. Yuan, and L. Huang, "Ultrafast Dynamic Microscopy of Carrier and Exciton Transport," Annu. Rev. Phys. Chem. **70**(1), 219–244 (2019).

Optics EXPRESS

9. Y. Zhu and J.-X. Cheng, "Transient absorption microscopy: Technological innovations and applications in materials science and life science," J. Chem. Phys. **152**(2), 020901 (2020).
10. S. Ahmed, X. Jiang, F. Zhang, and H. Zhang, "Pump–probe micro-spectroscopy and 2D materials," J. Phys. D: Appl. Phys. **53**(47), 473001 (2020).
11. E. S. Massaro, A. H. Hill, and E. M. Grumstrup, "Super-Resolution Structured Pump-Probe Microscopy," ACS Photonics **3**(4), 501–506 (2016).
12. G. Piland and E. M. Grumstrup, "High-repetition rate broadband pump-probe microscopy," J. Phys. Chem. A **123**(40), 8709–8716 (2019).
13. W. Choi, N. Choudhary, G. H. Han, J. Park, D. Akinwande, and Y. H. Lee, "Recent development of two-dimensional transition metal dichalcogenides and their applications," Mater. Today **20**(3), 116–130 (2017).
14. F. Kanal, S. Keiber, R. Eck, and T. Brixner, "100-khz shot-to-shot broadband data acquisition for high-repetition-rate pump–probe spectroscopy," Opt. Express **22**(14), 16965–16975 (2014).
15. N. M. Kearns, R. D. Mehlenbacher, A. C. Jones, and M. T. Zanni, "Broadband 2d electronic spectrometer using white light and pulse shaping: noise and signal evaluation at 1 and 100 khz," Opt. Express **25**(7), 7869–7883 (2017).
16. C. Schriever, S. Lochbrunner, E. Riedle, and D. J. Nesbitt, "Ultrasensitive ultraviolet-visible 20 fs absorption spectroscopy of low vapor pressure molecules in the gas phase," Rev. Sci. Instrum. **79**(1), 013107 (2008).
17. D. Uhl, L. Bruder, and F. Stienkemeier, "A flexible and scalable, fully software-based lock-in amplifier for nonlinear spectroscopy," Rev. Sci. Instrum. **92**(8), 083101 (2021).
18. G. Della Valle, M. Conforti, S. Longhi, G. Cerullo, and D. Brida, "Real-time optical mapping of the dynamics of nonthermal electrons in thin gold films," Phys. Rev. B **86**(15), 155139 (2012).
19. F. Balzer, H. Kollmann, M. Schulz, G. Schnakenburg, A. Lützen, M. Schmidtmann, C. Lienau, M. Silies, and M. Schiek, "Spotlight on excitonic coupling in polymorphic and textured anilino squaraine thin films," Cryst. Growth Des. **17**(12), 6455–6466 (2017).
20. S. Funke, M. Duwe, F. Balzer, P. H. Thiesen, K. Hingerl, and M. Schiek, "Determining the Dielectric Tensor of Microtextured Organic Thin Films by Imaging Mueller Matrix Ellipsometry," J. Phys. Chem. Lett. **12**(12), 3053–3058 (2021).
21. H. Chen, W. G. Herkstroeter, J. Perlstein, K.-Y. Law, and D. G. Whitten, "Aggregation of a Surfactant Squaraine in Langmuir-Blodgett Films, Solids, and Solution," J. Phys. Chem. **98**(19), 5138–5146 (1994).